IOPscience iopscience.iop.org

Home Search Collections Journals About Contact us My IOPscience

Theoretical studies of the angular correlation of positron annihilation in germanium

This article has been downloaded from IOPscience. Please scroll down to see the full text article.

1993 J. Phys.: Condens. Matter 5 3475

(http://iopscience.iop.org/0953-8984/5/21/012)

View the table of contents for this issue, or go to the journal homepage for more

Download details:
IP Address: 171.66.16.96
The article was downloaded on 11/05/2010 at 01:20

Please note that terms and conditions apply.

J. Phys.: Condens. Matter 5 (1993) 3475–3482. Printed in the UK

Theoretical studies of the angular correlation of positron annihilation in germanium

B K Panda and D P Mahapatra
Institute of Physics, Sachivalaya Marg, Bhubaneswar-751005, India

Received 25 June 1992, in final form 30 September 1992

Abstract. A pseudopotential formalism is applied to calculate the angular correlation of positron annihilation radiations (ACPAR) along the [100], [110] and [111] directions in Ge. The results are found to agree very well with the measured data. Calculations show that the ACPAR line shapes, particularly in the low-momentum region, are very much influenced by the detailed nature of bonding. Two-photon autocorrelation functions corresponding to the above symmetry directions are also presented and some interesting conclusions are drawn regarding positron–electron many-body correlation effects.

1. Introduction

Erskine and McGervey were the first to measure long-slit ACPAR lineshapes in Ge along the [100], [110] and [111] directions [1]. In the low-momentum region the lineshape for the [100] direction is found to be rather flat compared to the same for the other two directions. A close look at the remaining two spectra reveals a slightly peaking behaviour for the [111] direction. In addition, the profile along the [110] direction shows a sharp break in slope at 0.83 au. The authors employed a simplified Jones zone picture to explain this behaviour. However, using such a simplified picture it is not possible to understand the differences between the lineshapes observed in the low-momentum region. Later, Shulman and co-workers carried out a similar study at lower temperature with improved statistics [2]. They showed that at lower temperature the profiles for the [100] and [110] directions, instead of remaining flat, have small but prominent dips in the low-momentum region. The more recent data of Arifov and co-workers [3] also agree with the observations of Shulman and co-workers. The two-dimensional (2D) ACPAR measurement carried out at low temperature also confirmed this [2, 4]. In the case of Si and Ge [5, 6] long-slit ACPAR profiles for the [100] and [110] directions, calculated using the pseudopotential formalism, were found to reproduce these features. Using the same formalism, the nature of the long-slit ACPAR data along the [100] and [111] directions were explained in GaP [7] and GaSb [8]. As far as the 2D data are concerned, Chiba and Akahane carried out an LCAO calculation using an isotropic positron wavefunction and were somewhat successful in explaining the experimental data [9].

The effect of positron–electron many-body correlations on positron–electron pair momentum density was studied by Fujiwara and co-workers [10, 11]. Calculations show that there is an enhancement of momentum density at the zone face, with a reduction in the high-momentum components. It has been pointed out that enhancement and dehancement effects result, due to intraband and interband transitions of electrons respectively. In the case of Si, differences between calculated ACPAR line shapes and experimental data, particularly

0953-8984/93/213475+08$07.50 © 1993 IOP Publishing Ltd

along [110], very clearly show these effects. However, in the case of Ge the theoretical calculation [6] indicates some contradictory features. Although the theory is based on the independent particle model (IPM) approximation, the ACPAR line shape for the [110] direction shows a much sharper fall at the zone face compared to experimental data. Even in the high-momentum region theory shows much lower values, as if there is some kind of dehancement. This is supposed to be quite the opposite, since correlation effects have not been considered in the theory. This makes it very tempting to carry out a fresh calculation in Ge.

2. Theory

After entering into the solid the positron gets thermalized and attracts the surrounding electrons, whereby the electron density gets enhanced, and finally gets annihilated, emitting two photons. The probability of annihilation is proportional to the positron–electron pair momentum density $\rho^{2\gamma}(\boldsymbol{p})$:

$$\rho^{2\gamma}(\boldsymbol{p}) = \sum_{nk}^{\text{occ.}} \eta_n(\boldsymbol{k}) \left| \int \Psi_{nk}(\boldsymbol{r}) \Psi_+(\boldsymbol{r}) \exp(-\mathrm{i}\boldsymbol{p}\cdot\boldsymbol{r}) \mathrm{d}^3 r \right|^2. \tag{1}$$

Here, $\Psi_{nk}(\boldsymbol{r})$ and $\Psi_+(\mathbf{r})$ are the electron and positron wavefunctions respectively. Since the positron gets thermalized before annihilation, one takes its ground-state wavefunction at $\boldsymbol{k} = 0$; $\eta_n(\boldsymbol{k})$ is the occupation probability.

In long-slit experiments the coincidence counts for momentum p_z are given by

$$N(p_z) = \int_{-\infty}^{\infty} \int_{-\infty}^{\infty} \rho^{2\gamma}(\boldsymbol{p}) \mathrm{d}p_x \mathrm{d}p_y. \tag{2}$$

Following Berko [12] the two-photon autocorrelation function (AF) is defined as the Fourier transform of $\rho^{2\gamma}(\boldsymbol{p})$:

$$B^{2\gamma}(\boldsymbol{r}) = \int \rho^{2\gamma}(\boldsymbol{p}) \exp(\mathrm{i}\boldsymbol{p}\cdot\boldsymbol{r}) \mathrm{d}^3 p. \tag{3}$$

In the pseudopotential formalism the pseudo-wavefunctions are nodeless, because the core-orthogonalization term is neglected, and are given by

$$\Psi_{nk}(\boldsymbol{r}) = \left(\frac{1}{\Omega}\right)^{1/2} \sum_{\boldsymbol{G}} C_{nk}(\boldsymbol{G}) \exp[\mathrm{i}(\boldsymbol{k}+\boldsymbol{G})\cdot\boldsymbol{r}]. \tag{4}$$

The positron wavefunction was solved with the ionic potential taken in the point-core approximation [6, 13]. With the potential diverging at the ion core region the wavefunction is expected to need a lot of plane waves in order to converge. However, the situation is simplified because of the fact that the positron gets pushed away from the ion core region into the interstitial positions, with its wavefunction vanishing at the ion core. This smooth structure of the positron wavefunction, which has no oscillations in the ion core region, lends itself very well to a representation in terms of a relatively small number of plane waves:

$$\Psi_+(\boldsymbol{r}) = \left(\frac{1}{\Omega}\right)^{1/2} \sum_{\boldsymbol{G}} A(\boldsymbol{G}) \exp(\mathrm{i}\boldsymbol{G}\cdot\boldsymbol{r}). \tag{5}$$

Using (4) and (5), the pair momentum density can be derived as

$$\rho^{2\gamma}(\boldsymbol{p}) = \frac{1}{\Omega}\sum_{nk}\eta_n(\boldsymbol{k})\sum_{G}\left|\sum_{G'}C_{nk}(G')A(G'-G)\right|^2\delta(\boldsymbol{p}-\boldsymbol{k}-\boldsymbol{G}). \tag{6}$$

The evaluation of $B^{2\gamma}(\boldsymbol{r})$ using $\rho^{2\gamma}(\boldsymbol{p})$ from (6) is straightforward. From a knowledge of $B^{2\gamma}(\boldsymbol{r})$ along a given crystallographic direction one can evaluate $N(p_z)$ for that direction through a Fourier inversion.

In the present case the non-local pseudopotential parameters of Chelikowsky and Cohen [14] were used to calculate the electron pseudo-wavefunctions. For electron and positron wavefunctions we have taken 100 and 300 plane waves respectively. The summation over the occupied $\boldsymbol{k}$-space was carried out using the sixty-point scheme of Chadi and Cohen [15]. The core contributions were evaluated following Yongming and co-workers [16] and added to the valence profiles. For comparison, both the theoretical and experimental data were normalized to unity.

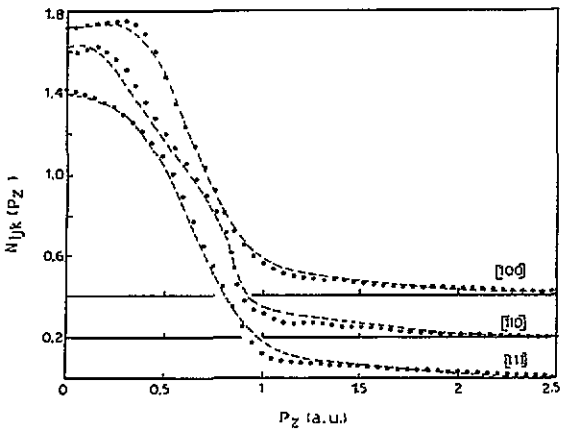

Figure 1. Experimental (●) and theoretical (– – –) ACPAR lineshapes along the [100], [110] and [111] directions of Ge.

3. Results and discussions

3.1. ACPAR lineshapes

The calculated ACPAR lineshapes for Ge along the three principal symmetry directions, namely [100], [110] and [111], are shown in figure 1. The corresponding experimental data [2] are also shown in the same figures. The theory is seen to reproduce more or less the experimental features. In the low-momentum region lineshapes for [100] and [110] are seen to be flatter than the same for the [111] direction. Along the [110] direction the lineshape shows a sharp break in slope around $q = 0.83$ au. As shown earlier, this break in slope can be understood in terms of the geometry of the occupied volume in k space, i.e. the Jones zone [1]. The failure of the Jones zone model is primarily due to the consideration only of an occupied volume in k space and the neglect of the detailed nature of the underlying wavefunction. This is in agreement with the findings of Nara and co-workers, who have concluded from their Compton profile (CP) anisotropy calculations in

most of the semiconductors that the low-momentum region of the CP is dominated by the nature of bonding orbitals [17].

In order to see how the low-momentum behaviour is influenced by the bonding orbitals we shall follow a line of analysis that is due to Pattison and co-workers [18]. In the case of Si they have shown that along [111] there is a $(3p, 3p)\sigma$ bond at the first bond length, and the interaction of the second neighbour $(3p, 3p)\sigma$ bonds is equivalent to introducing a $(3p, 3p)\pi^*$ bond along [110] between neighbouring atoms. Similarly, in Ge there is a $(4p, 4p)\sigma$ bond at the first bond length and a $(4p, 4p)\pi^*$ bond at the second bond length. As a result of this, there is a $(4p, 4p)\sigma$ bond along the [111] direction and an admixture of $(4p, 4p)\sigma$ and $(4p, 4p)\pi^*$ bonds along the [110] direction. Similarly, one can also find that [100] direction also contains an admixture of $(4p, 4p)\sigma$ and $(4p, 4p)\pi^*$ bonds. In the low-momentum region a σ bond is expected to result in a relatively sharper profile, as compared to the same for an admixture of σ- and π-type bonding. With a π-type contribution there can even be a dip at $q = 0$. This has been very clearly demonstrated in case of graphite [19, 20]. Similarly, in the present case the $(4p, 4p)\sigma$ bond makes the profile sharply peaked along the [111] direction and the admixture of $(4p, 4p)\sigma$ and $(4p, 4p)\pi^*$ bonds results in a dip in the low-momentum region for both [100] and [110] directions.

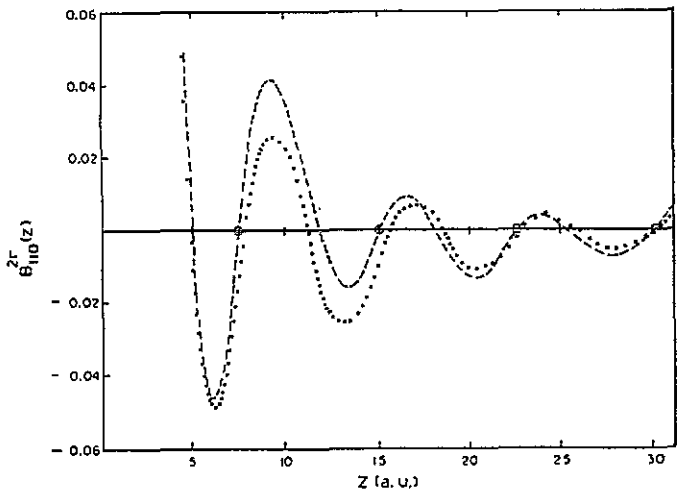

Figure 2. Experimental (●) and theoretical (– – –) two-photon AF for Ge along the [110] direction. The circles show the lattice positions along this direction.

The experimental lineshape for the [110] direction is seen to have a sharper slope close to the zone face (figure 1) than the theoretical one. In addition, in the high-momentum region experimental data are seen to lie below the theoretical data. The sharp slope is due to enhancement effects arising out of positron–electron many-body correlations, which also dehance the high-momentum components [10]. This feature is also shown in the recent experimental $\rho^{2\gamma}(p)$ by Weimin and co-workers [21].

The theory fails to reproduce the Umklapp annihilation components seen at 1.66 au in the experimental data for the [110] direction. This failure can be attributed to the neglect of core orthogonalization effects. In case of aluminium an OPW calculation was found to generate Umklapp components, while a pseudopotential calculation failed to reproduce it [22]. Core-orthogonalized band wavefunctions might reproduce the Umklapp components.

3.2. Two-photon AF and their anisotropies

Figure 2 shows both experimental and present theoretical 2γ AF for Ge along the [110]

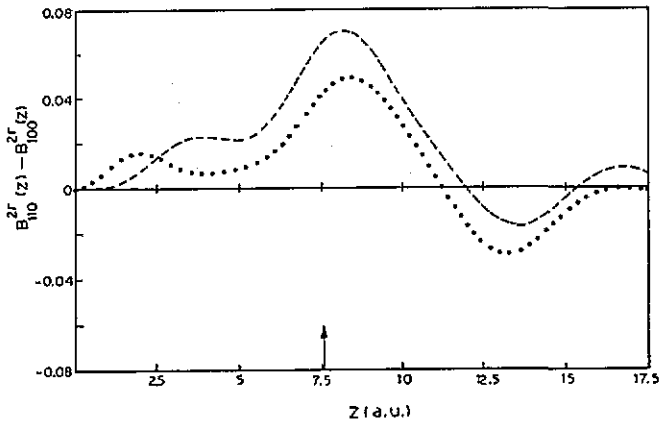

Figure 3. Experimental (●) and theoretical (– – –) AF anisotropy between the [110] and [100] directions of Ge. The arrow shows the position of the second neighbour.

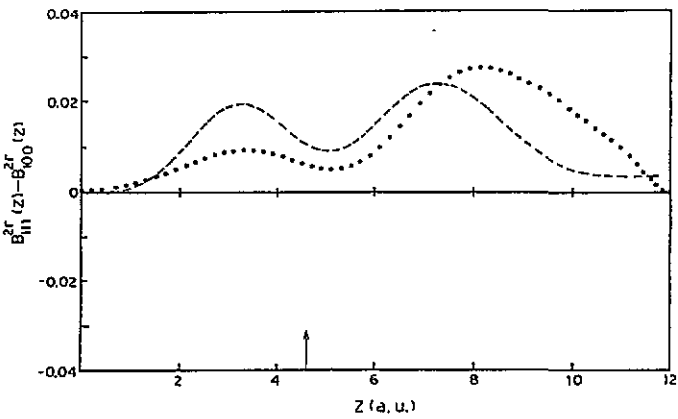

Figure 4. Same as in figure 3, but between [111] and [100] directions of Ge. The arrow shows the position of the first neighbour.

direction. As has been shown earlier [23], for a system with filled bands, the AF derived from CP data along a given direction is expected to produce zero passages at lattice sites. But the zero positions in the experimental $B^{2\gamma}(z)$ are seen to be shifted to the right of the expected lattice positions [24]. Compared to this, the same in the present theoretical curve are seen to reproduce lattice positions exactly. The positron wavefunction does not change the zero positions. This is expected, since the present theory does not take into account the positron–electron correlation potential and many-body enhancement or dehancement effects. Recently, Yongming and co-workers [25] have given a method to calculate a positron–electron product wavefunction solving the Schrödinger equation with a combined positron–electron potential. In their calculation on aluminium they have shown that there are two kinds of correlation effects. The isotropic bulging of the experimental two-dimensional ACPAR lineshape between 2.5–6.0 mrad is primarily due to an enhancement effect, taken care of in most of the theories developed for the purpose. In addition to this there is also another anisotropic enhancement effect, resulting in small structures around 3.0 and 6.0 mrad that arise through the correlation potential. Using their potential, one of the present authors, in a recent work on aluminium [26], has calculated the positron–electron product wavefunction and has shown that there is no zero shift in the derived AF as compared to the results obtained using the IPM. The anisotropic enhancement effects that result in small structures,

as mentioned earlier, do not result in any shifting of the zeros in the AF. However, with inclusion of positron–electron correlation effects through an enhancement factor [27], it was seen that the zero positions changed and agreed with the experimental data. Yongming and co-workers have also carried out such a calculation in Si [28]. We have again used their potential to carry out an AF calculation in Si. Here, also, we did not find any change in the zero crossings as compared to the IPM results. This makes us feel that the small differences existing between the zero crossings in the AF derived from theoretical and the experimental data arise from the non-inclusion of positron–electron many-body enhancement and dehancement effects, rather than the positron–electron correlation potential.

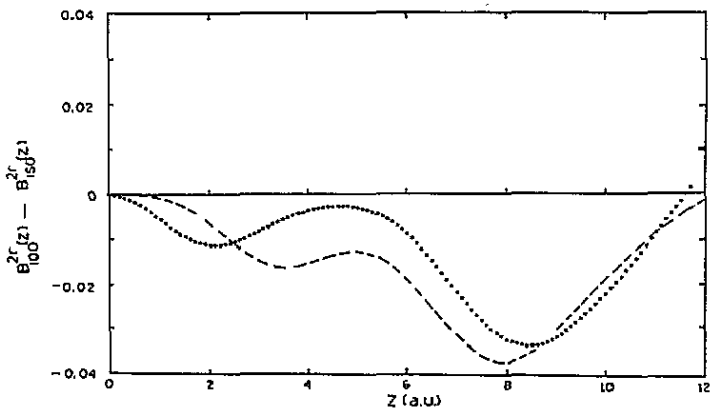

Figure 5. Experimental (●) and theoretical (– – –) AF anisotropy along the [100] directions. $B^{2\gamma}_{iso}(z)$ is calculated as $B^{2\gamma}_{iso}(z) = (6B^{2\gamma}_{100}(z) + 12B^{2\gamma}_{110}(z) + 8B^{2\gamma}_{111}(z))/26$.

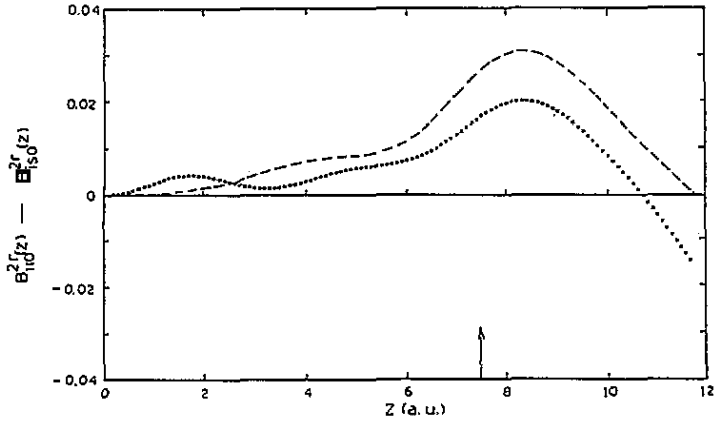

Figure 6. Same as in figure 5, but for the [110] direction. The position of the arrow is the same as in figure 3.

However, a close inspection tells us that the positron–electron many-body correlation effects change the zero positions in the opposite way as compared to aluminium. This clearly suggests that, in the case of Ge, a different form of enhancement factor is necessary to explain the experimental zeros. In aluminium, positron–electron correlation effects are known to affect only the lower-order zeros [26, 29]. This conclusion is based on the fact that only the lower-order zeros, as obtained from an IPM calculation without inclusion of correlation effects through an enhancement factor, show deviations from experiment. The

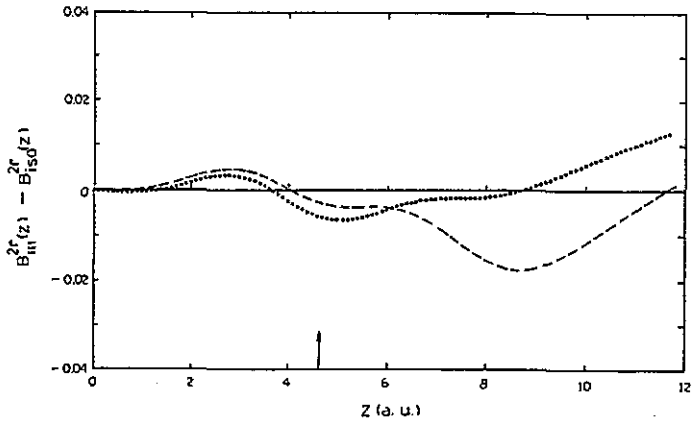

Figure 7. Same as in figure 5, but for the [111] direction. The position of the arrow is the same as in figure 4.

higher-order zero positions are relatively less affected. In case of Ge the situation is also quite similar (figure 2).

Bonding effects can be very clearly seen in position space by looking at the AF anisotropy. For instance, the CP $B_{111} - B_{100}$ anisotropy shows a prominent dip at the first bond length corresponding to the σ bond along the [111] direction. As has been already shown, the second-neighbour interaction results in a π^* bond along [110]. This is also reflected in a prominent peak at the second-neighbour bond length in $B_{110} - B_{100}$. This happens because [100] direction with atoms far apart is a non-bonding direction. The $B^{2\gamma}_{110} - B^{2\gamma}_{100}$ and the $B^{2\gamma}_{111} - B^{2\gamma}_{100}$ anisotropies for Ge are shown in figures 3 and 4, respectively. In figure 3 one can notice a peak close to 7.5 au which, in analogy with corresponding CP data, may be thought of as coming from second-neighbour π-bond effects. Similarly, in figure 4 one can notice a minimum around 5.0 au which, again, can be thought of as coming from the dip in the CP data and which, as has been shown earlier, arises due to the first-neighbour σ-bond. However, one has to exercise some caution before making such statements. This is because, unlike the CP case, [100] is not a non-bonding direction in the sense that positron localization effects are more important for this direction. Since the $B^{2\gamma}_{111} - B^{2\gamma}_{100}$ anisotropy showed a minimum at the first bond length instead of a negative dip, as in the CP case, it was tempting to explore the nature of the anisotropic $B^{2\gamma}(z)$ along various directions. For this one needs to subtract from $B^{2\gamma}(z)$ along each direction an isotropic part. In figures 5–7 we have presented these data for the [100], [110] and [111] directions, respectively. One can see with positrons that the [111] direction plays the role of a non-bonding direction (figure 7). In fact, figures 4 and 5 essentially show the same data. Unlike the CP results, the [100] direction behaves like a bonding direction. The dip at 8.0 au (figure 5) is primarily due to positron localization effects rather than any bonding effects. The nature of anisotropy along the [110] (figure 6) direction remained same as in figure 3. All the above conclusions, one must not forget, are derived from results obtained from an IPM calculation. The inclusion of positron–electron correlation effects will only result in a slight change in the AF, which is not expected to change the AF anisotropy drastically.

4. Conclusion

In the present paper we have reported ACPAR lineshapes calculated within the pseudopotential formalism employing the IPM. The results are found to be in reasonable agreement with

available experimental data. In the low-momentum region the lineshapes are found to be strongly influenced by the actual symmetry of the orbitals taking part in bonding. Experimental data show prominent enhancement and dehancement effects, which are not seen in the theoretical data due to the neglect of correlation effects. Fourier-transformed ACPAR data also show how the zero passages are affected due to the neglect of correlation effects. In fact, we feel that the inclusion of an enhancement factor based on the jellium model may not result in a shift of the zeros in a correct direction. The anisotropic AF along the [111] direction is significantly different from that obtained from CP data.

References

[1] Erskine J C and McGervey J D 1966 *Phys. Rev.* **151** 615
[2] Shulman M A, Beardsley G M and Berko S 1975 *Appl. Phys.* **5** 367
[3] Arifov P U, Arutyunov N Yu, Trashchakov V Yu and Abdurasuev Z R 1983 *Sov. Phys. Semicond.* **17** 1232
[4] West R N, Meyers J and Walters P A 1981 *J. Phys. E: Sci. Instrum.* **14** 478
[5] Stroud D and Ehrenreich H 1968 *Phys. Rev.* **171** 399
[6] Aourag H, Belaidi A, Kobayashi T, West R N and Khelifa B 1989 *Phys. Status Solidi* b **155** 191
[7] Panda B K, Mahapatra D P and Padhi H C 1991 *Phys. Status Solidi* b **167** 133
[8] Panda B K, Mahapatra D P and Padhi H C 1992 *Phys. Status Solidi* b **169** 89
[9] Chiba T and Akahane T 1989 *Positron Annihilation* ed L Doriken-Vanpraet, M Dorikens and D Segers (Singapore: World Scientific) p 674
[10] Fujiwara K, Hyodo T and Ohyama J 1972 *J. Phys. Soc. Japan* **33** 1047
[11] Fujiwara K and Hyodo T 1973 *J. Phys. Soc. Japan* **35** 1133
[12] Berko S 1983 *Positron Solid State Physics* ed W Brandt and A Dupasquier (Amsterdam: North-Holland) p 64
[13] Aourag H, Khelifa B, Belaidi A, Tedjer A, Rezki M and Gamoudi M 1990 *Phys. Status Solidi* b **160** 201
[14] Chelikowsky J R and Cohen M L 1976 *Phys. Rev.* B **14** 556
[15] Chadi D J and Cohen M L 1973 *Phys. Rev.* B **8** 5747
[16] Lou Yongming, Johansson B and Nieminenm R M 1991 *Phys. Scri.* **43** 123
[17] Nara H, Kobayashi T and Shindo K 1984 *J. Phys. C: Solid State Phys.* **17** 3967
[18] Pattison P, Hansen N K and Schneider J R 1981 *Chem. Phys.* **59** 231
[19] Lou Yongming, Johansson B and Nieminen R M 1991 *J. Phys.: Condens. Matter* **3** 2057
[20] Lou Yongming, Johansson B and Nieminen R M 1991 *J. Phys.: Condens. Matter* **3** 1699
[21] Weimin Liu, Berko S and Mills A P Jr private communication
[22] Mader J, Berko S, Krakauer H and Bansil A 1976 *Phys. Rev. Lett.* **37** 1232
[23] Pattison P and Schneider J R 1978 *Solid State Commun.* **28** 581
[24] Berko S, Farmer W S and Sinclair F 1982 *Positron Annihilation* ed P G Coleman, S C Sharma and L M Diana (Amsterdam: North-Holland) p 319
[25] Lou Yongming, Nieminen R M and Johansson B 1991 *J. Phys.: Condens. Matter* **3** 163
[26] Panda B K 1992 *Phys. Status Solidi* b **170** 481
[27] Mijnarends P E and Singru R M 1979 *Phys. Rev.* B **19** 6038
[28] Lou Yongming, Johansson B and Nieminen R M 1991 *Phys. Scri.* **43** 123
[29] Dlubek G and Gerber W 1990 *Phys. Status Solidi* b **161** K81